An Integrative 3D printing method for rapid additive manufacturing of a capacitive force sensor

An Integrative 3D Printing Method for Rapid Additive Manufacturing of a Capacitive Force Sensor

G.D. Liu[1], C.H. Wang[1], Z.L. Jia[2] and K.X. Wang[1]

[1] Institute of Sensors, Signals and Systems, School of Engineering & Physical Sciences, Heriot-Watt University Edinburgh EH14 4AS, UK
[2] Center for Advanced Measurement Science, National Institute of Metrology, Beijing 100029, China

E-mail: g.liu@hw.ac.uk, c.wang@hw.ac.uk

Received xxxxxx
Accepted for publication xxxxxx
Published xxxxxx

Abstract

With the rapid development of the three-dimensional printing (3D Printing) technique, several electronic devices have been fabricated by 3D printing. Compared with the traditional MEMS manufacturing processes, the 3D printing technique provides a convenient method to meet the customers' personalized demands. However, the applications of 3D printing are restricted by the electrically insulating properties of the commonly used polymers. Besides, additional alignment and assembling processes are still indispensable to fabricate the MEMS devices with geometrically complex structures using the conventional 3D printers. In order to solve these problems, an integrative 3D printing approach for rapid manufacturing is presented in this paper. With a triple-extruder 3D printer, the electrically insulating PLA filament, the electrically conductive PLA filament, and the soluble HIPS filament can be printed alternately in the 3D printing process. As an application of the method, a capacitive force sensor with a relatively complex suspended beam-plate structure was fabricated in a one-step 3D printing process without using any additional metallization process, unloading-reloading filament process, alignment process, and assembling process. With a good dynamic performance, the 3D printed force sensor was used to monitor human's blood pulse. The results show that the integrative 3D printing method has potential to meet the emerging requirement for manufacturing of MEMS devices for personalized applications.

Keywords: integrative 3D printing; force sensor; personalized customization; conductive filament; sacrificial layer

1. Introduction

In recent decades, the silicon-based MEMS (Micro Electromechanical System) technique has been extensively used in fabrication of a variety of transducers, which is attributed to its advantages of mass production, high precision, and compatible with the normal silicon-based IC process [1-6]. However, the traditional manufacturing processes usually take several months and the types of products are usually limited, which restricts their applications in the field of personalized customization. The three-dimensional printing (3D Printing) technique provides a convenient solution to fulfill the customers' personalized requirements. 3D printing is a promising distributed manufacturing technique [7], which is also known as additive manufacturing (AM). Compared with the traditional subtractive method, the additive

manufacturing method can reduce time and save materials since it doesn't need to remove materials from a block in the fabrication process. Furthermore, additive manufacturing has the ability to fabricate geometrically complex structures. Depending on the manufacturing principles, 3D printing techniques can be divided into fused deposition modeling (FDM), stereolithography (SLA), selective laser sintering (SLS), inkjet printing, laminate object manufacturing (LOM) and so on [8-16]. Compared with other methods, FDM is one of the most commonly used techniques due to its simple principle and low material cost. In the FDM printing process, the melted material is deposited on the platform layer by layer to build up the 3D object [17-20]. A variety of thermoplastic materials such as acrylonitrile butadiene styrene (ABS), polylactic acid (PLA), high impact polystyrene (HIPS), polycarbonate (PC), nylon, polyvinyl alcohol (PVA), and polyethylene terephthalate (PET) are usually used as filament materials for FDM printing [21-25]. Among these materials, PLA has been widely used because it is an environmentally material with better stability in heat shrinkage than other thermoplastics such as ABS [26-28].

Although several electronic devices have been produced using 3D printing [29-37], there are many steps in the fabrication process. Since most of the thermoplastics are not electrically conductive materials. an additional metallization process has to be applied, which complicates the fabrication process. Valentina Zega *et al.* [38] reported a 3D-printed z-axis accelerometer. The mechanical structure of the accelerometer was made by 3D printing and the electrodes were fabricated by electroless deposition and electrolytic deposition of copper (Cu). Since the wet-metallization method is difficult to deposit the copper selectively, additional PET sheets had to be placed between the electrodes of the parallel-plate capacitors to provide electrical isolation. Conductive ink-jet printing is another metallization method for 3D printed polymer structures. Jacob J. Adams *et al.* [39] reported an antenna, which was fabricated by printing concentrated silver nanoparticle ink onto a glass hemisphere. After printing, the sample was heated at 550ºC for 3 hours to form the conductive silver traces. L-M Faller *et al.* [40] reported a force sensor, which was fabricated based on 3D printed ceramic diaphragms. The electrodes were fabricated by inkjet printing a silver nanoparticle ink. After printing, the silver ink was sintered at 300ºC for 1 hour. Compared with the wet-metallization method, the inkjet printing method based on conductive inks can deposit the metal films selectively. However, the sintering temperatures of the silver inks are usually above 150ºC, which is too high for the 3D printed polymers. The warping deformation during the sintering process can cause device performance degradation. Ghazali *et al.* [41] reported 3D printed structures for RF (radio frequency) circuits. A thin titanium (Ti) film and a copper film were deposited on the 3D printed substrates by sputtering. After that, a damascene-like process was used to pattern the metal films. Jose Marques Hueso *et al.* [42] reported a selective electroless copper deposition method. After exposing, the reduction of silver nanoparticles on the surface of the 3D printed sample from photosensitive silver chloride (AgCl) was used as a seed layer for electroless copper plating. Both the metal sputtering process and the exposure process are relatively complex.

In recent years, it has been reported that some thermoplastic filaments with conductive fillers, such as carbon black, carbon nanotubes, and graphene, exhibit conducting properties [43-48]. Since the conductive thermoplastic filaments are compatible with the normal FDM 3D printing process, they provide a convenient solution for printing the electrically conducting components of the electronic devices. Simon J. Leigh *et al.* [49] reported many applications of the carbon black polymer composites on 3D printed sensors. J. R. McGhee *et al.* [50] reported the strain sensing characteristics of the 3D printed conductive PLA and ABS. With the conductive polymer composites, several electronic components and circuits were produced using FDM 3D printers without using additional sputtering machines or exposure machines [41, 42]. Moreover, the conductive polymer printing exhibits potential to be applied in selective electroplating for high conductive devices [51, 52]. Although the conductive components of some electronic devices, such as strain sensors and antennas, have been 3D printed using the conductive filaments, the geometric structures of these devices were relatively simple. While complex suspended structures are usually adopted in MEMS devices [1, 38]. In the bottom-up fabrication process, the upper suspended structures cannot be directly 3D printed on the under substrates without supporters. Since most of the FDM 3D printers have only one extruder, the components of the MEMS devices are usually printed separately and then manually assembled together [38]. Hence, additional alignment process and assembling process are still needed to fabricate the MEMS devices with geometrically complex structures using the conventional 3D printers.

In this paper, we report an integrative 3D printing method for fabrication of a capacitive force sensor, which has a relatively complex suspended structure. With an electrically insulating PLA filament, an electrically conductive PLA filament, and a soluble HIPS filament, the force sensor was fabricated using a triple-extruder 3D printer in a one-step printing process in approximately 35 minutes without any additional metallization process, unloading-reloading filament process, alignment process, and assembling process. The 3D printed force sensor has been successfully fabricated and applied in monitoring the blood pulse.

2. Materials and methods

2.1 Materials

The carbon black-based electrically conductive PLA filament was purchased from Proto-Pasta. The resistivity was 15 Ω·cm. The HIPS filament and the D-Limonene solvent were bought from RS Components Ltd. The diameters of all filaments were 1.75 mm. The 3D printer Creatbot® DX was supplied by Suwei Electronic Technology Co., Ltd. The diameter of the nozzle of the 3D printer was 0.4 mm. The capacitive readout IC MS3110 was obtained from Irvine Sensors. The MS3110 has a capacitance resolution of 4.0 aF/rtHz and can provide an output voltage proportional to the capacitance change.

2.2 Characterization

The surface morphologies of the carbon black-based PLA structure were observed using a scanning electron microscope (SEM). It can be seen from the SEM images in Fig. 1a and Fig. 1b, the 3D printed conductive structure has a smooth surface with few defects, which ensures stable electrical conductivity. To verify the conductive effect, carbon black-based PLA interconnections were 3D printed on the normal PLA substrates. As shown in Fig. 1c and Fig. 1d, by connecting to the electrically conductive PLA traces, the LEDs were successfully operated. Therefore, the electrically conductive PLA filament material can be employed to fabricate the electrodes and interconnections for 3D printed electronic devices.

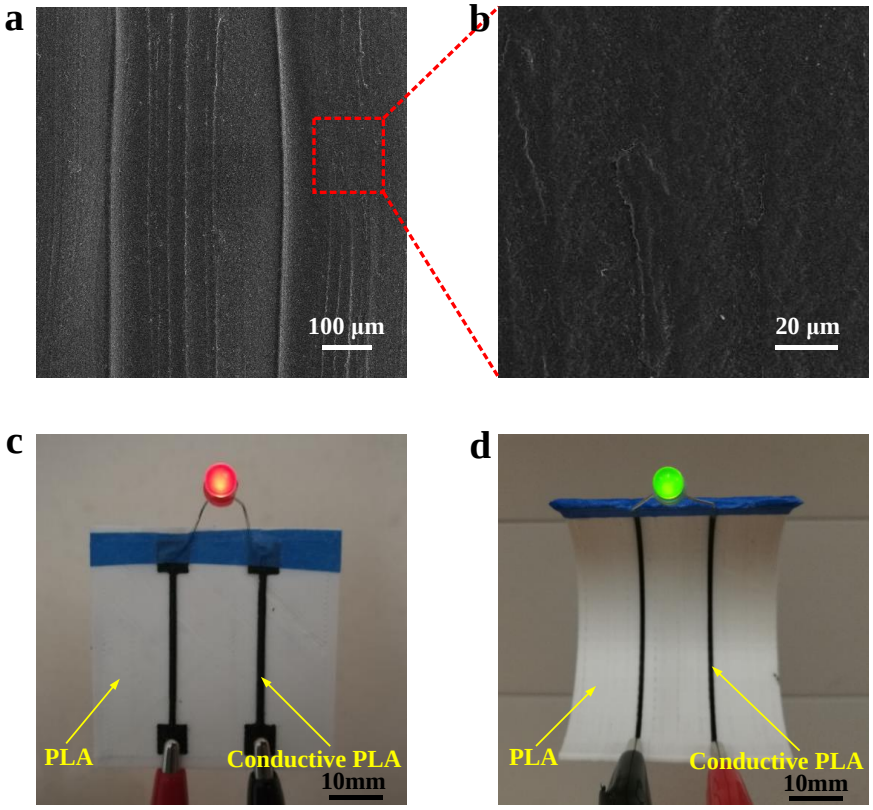

Figure 1. SEM images of the carbon black-based PLA structure and photographs of 3D printed conductive interconnects. (a) SEM image of the carbon black-based PLA object. (b) SEM image of the carbon black-based PLA object with higher magnification. (c) An LED was operated successfully by connecting to a flat 3D printed circuit. (d) An LED was operated successfully by connecting to a cambered 3D printed circuit.

2.3 Design

As shown in Fig. 2a, the capacitive force sensor consists of a top plate, a top electrode, a spacer, a bottom electrode, and a bottom plate. In the top plate, a movable plate is suspended by four beam springs and form a beam-plate structure. Each beam spring has several connected L-shape beams. Thus, the movable plate and the fixed bottom plate form a variable parallel-plate capacitor. The initial capacitance (C_0) of the variable capacitor can be expressed as [53]

$$C_0 = \varepsilon \frac{A}{d} \quad (1)$$

where ε is the permittivity of the media between two parallel plates, A is the effective area of the movable plate, and d is the gap distance between the top plate and the bottom plate. When

an external force is applied on the surface of the top plate, the plate will move towards the bottom plate thereby decreasing the gap distance between the two parallel plates and increasing the capacitance. The capacitance under the external force (C_1) can be expressed as

$$C_1 = \varepsilon \frac{A}{(d - x)} \quad (2)$$

where x is the displacement of the movable plate. Therefore, the external force can be measured by detecting the capacitance changes (C_1 - C_0). Fig. 2c shows the top view of the beam-plate structure. The long beam length (BL1) was 12 mm, the beam width (BW) was 0.4 mm, the short beam length (BL2) was 0.8 mm, the plate width (MW) was 12 mm, the beam thickness (BT) was 1.2 mm, and the gap distance was 2.7 mm.

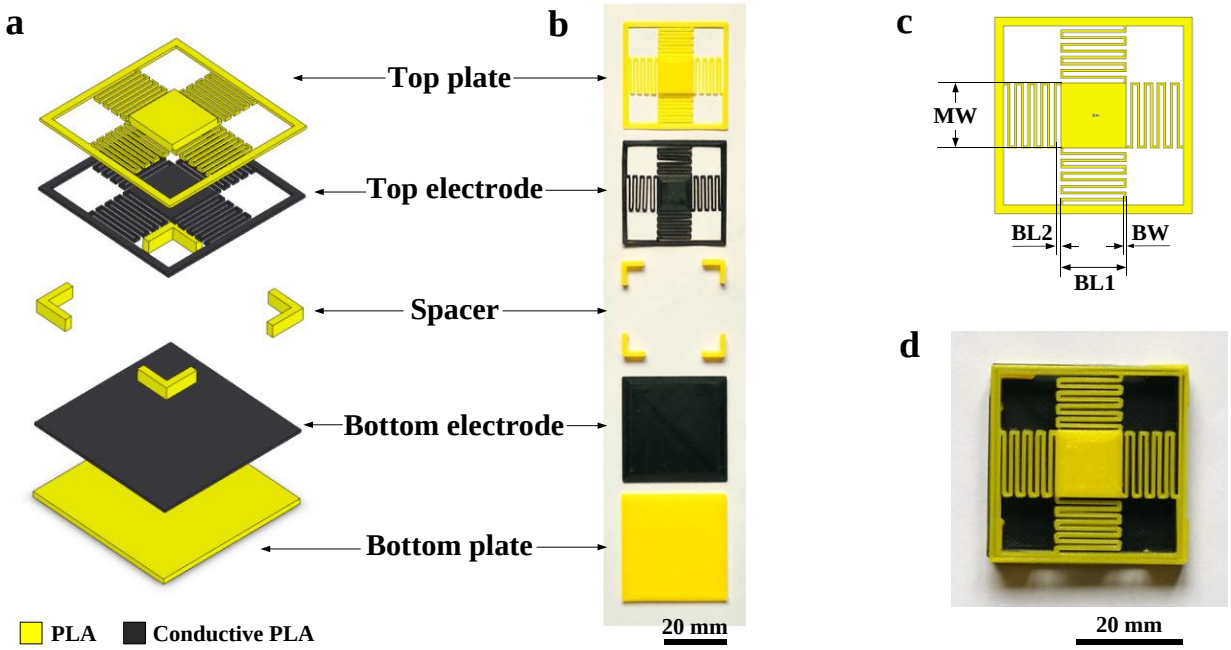

Figure 2. Schematic diagrams and photographs of a capacitive force sensor fabricated using a traditional multi-step printing method. (a) Exploded view of the functional layers. (b) Photograph of the 3D printed components of the force sensor. (c) Top view of the beam-plate structure. (d) Photograph of the 3D printed force sensor after assembling.

Since the shape of the beam spring has a significant influence on the displacement of the plate, finite element method (FEM) was used to analyze the relationship between the shape of the beam spring and the displacement of the plate. FEM models of the beam-plate structure with different beam spring shapes were built using the FEM software ANSYS. The number of the L-shape beam was varied between 1 and 8. Other geometric parameters in different models were maintained. When a pressure (P) of 30 Pa was applied on the surface of the top plate, the relationship between the number (N) of L-shape beam and the displacement of the plate is shown in Fig. 3a. It can be seen that the displacement of the plate increases with the number of L-shape beam. Hence, the sensitivity of the force sensor can be improved by increasing the number of L-shape beam. Considering both the sensitivity and the dimension of the device, the number of the L-shape beam was set to 8. In order to analyze the influence of the beam thickness on the displacement of the plate, the beam thickness was varied between 1.2 mm and 2.2 mm. Other parameters were maintained. As shown in Fig. 3b, the displacement of the plate decreases with the beam thickness increasing. Considering both the sensitivity and the reliability of the beam-plate structure, the beam thickness was set to 1.2 mm. Fig. 3c shows a linear relationship between the external force and the displacement of the plate, which indicates the beam-plate structure exhibits good spring-like properties. When an external pressure of 30 Pa was applied on the surface of the top plate, the deformation of the plate in the z-axis direction is shown in Fig. 3d.

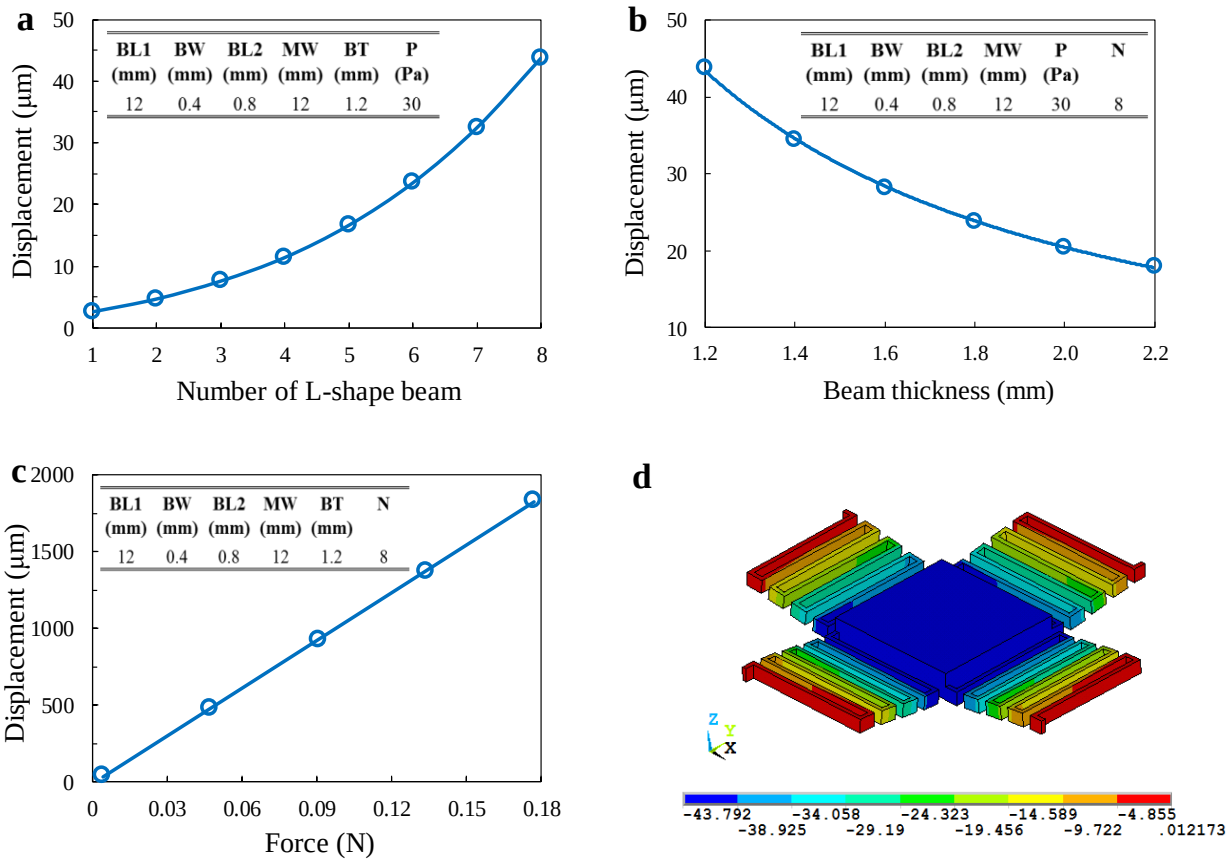

Figure 3. FEM simulation results of the beam-plate structure. (a) Relationship between the number of L-shape beam and the displacement of the plate. (b) Relationship between the beam thickness and the displacement of the plate. (c) Relationship between the external force and the displacement of the plate. (d) Deformation of the plate in the z-axis direction under an external pressure of 30 Pa.

2.4 3D printed force sensor based on a multi-step printing method

Since most of current FDM 3D printers have only one extruder, the five components of the capacitive force sensor have to be 3D printed separately and then manually assembled together. A force sensor was fabricated using this multi-step printing method for prototype verification. The components of top plate, spacer and bottom plate were 3D printed using a normal PLA filament. The printing temperature was 190ºC and the fill rate was 100%. After that, the normal PLA filament was unloaded from the extruder. Then the carbon black-based PLA filament was uploaded and used to print the components of top electrode and bottom electrode. The printing temperature was 230ºC and the fill rate was 100%. Fig. 2b shows the photograph of the 3D printed components of the force sensor. After printing, the components were aligned and then assembled together using a super glue at room temperature. Fig. 2d shows the photograph of the 3D printed capacitive force sensor.

2.5 3D printed force sensor based on an integrative 3D printing approach for rapid manufacturing

Although it has been demonstrated that the conventional metallization processes such as electroplating, spraying, sputter, evaporation, and inkjet printing can be replaced by the new method of conductive PLA 3D printing in some applications, additional processes such as unloading-reloading filament, alignment and assembling process of the individual components are still indispensable thereby decreasing the manufacturing efficiency. In order to overcome this shortcoming, we demonstrate an integrative 3D printing method using a triple-extruder 3D printer and the associated fabrication processes. Fig. 4a shows a photograph of the triple-extruder 3D printer. It can be seen that the left extruder was loaded with the normal PLA filament, the right extruder was loaded with the carbon black-based PLA filament, and the middle extruder was loaded with the HIPS filament which was used as a sacrificial material. Therefore, the three different filaments can be printed in a one-step 3D printing process without using additional unloading-reloading filament and

metallization process. Besides, since the three extruders have been aligned, the three different filaments can be 3D printed alternately on the exact location without needing an additional alignment process.

In the 3D model of the capacitive force sensor shown in Fig. 2a, the top plate and the bottom plate are separated in the vertical direction by a spacer layer thereby forming a suspended structure. However, the air gap cannot be produced in the 3D printing process since in the bottom-up printing process, the upper structure cannot be directly 3D printed on the under structure without supporters. Although the supporters can be 3D printed using the same filament material as the structural frame [54], it still needs to remove the supporters manually. Especially for small-size MEMS devices, the removal of the supporters is very difficult. In order to solve this problem, as shown in Fig. 4b, a 3D printed HIPS structure provides a temporary supporter for the upper structure, which plays the role of sacrificial layer. After printing, the temporary HIPS supporter can be selectively removed by the environmentally friendly solvent of D-Limonene, while the functional layers won't be affected [55]. Therefore, with the HIPS sacrificial layer, the upper structure can be directly 3D printed on the under structure without using additional assembling process. After 3D printing, the HIPS sacrificial layer can be selectively dissolved in D-Limonene without manual removal. It should be pointed out that the HIPS sacrificial layer was not a solid structure. In order to reduce the amount of the HIPS filament and make the solvent of D-Limonene dissolve the HIPS sacrificial layer easily after printing, the inner of the HIPS supporter was designed as a grid structure. Only the top surface and the bottom surface of the HIPS supporter were solid planes.

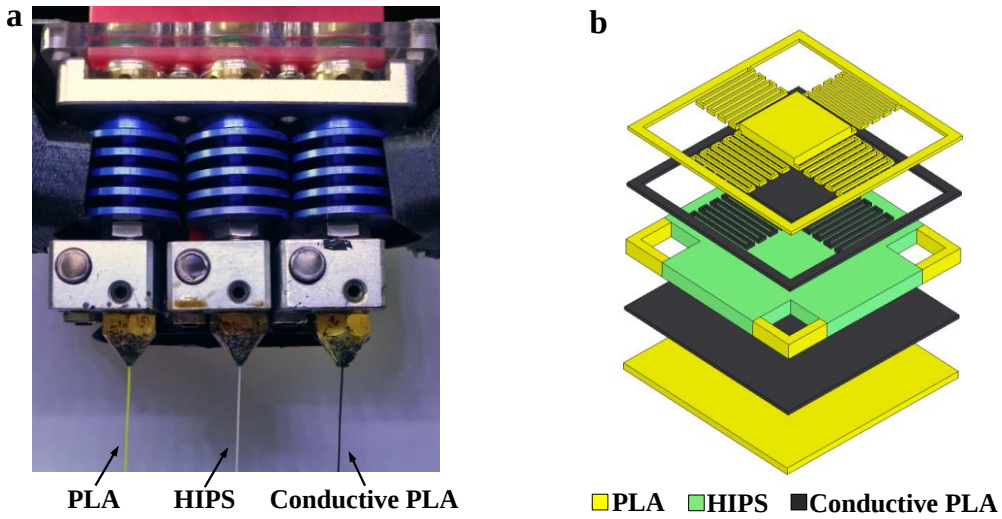

Figure 4. Photograph of the triple-extruder 3D printer and 3D model slicing. (a) Photograph of the triple-extruder 3D printer. (b) Exploded view of the functional layers of the capacitive force sensor for integrative 3D printing.

The CAD model of the capacitive force sensor was created using the 3D modeling software Solidworks and saved as a stereolithography (STL) file. The 3D model in the STL file was sliced into thin layers and exported as a G-code file using a slicing software CreatWare. Then the G-code file was transferred to the triple-extruder 3D printer to print the force sensor. In the integrative 3D printing process depicted in Fig. 5, the three extruders of the 3D printer worked alternately and fabricated the 3D model through a bottom-up layer-by-layer process. With good mechanical properties and electrically insulating properties, the normal PLA filament was extruded at a temperature of 190ºC using the left extruder to print the bottom plate, top plate, and spacer. The carbon black-based conductive PLA filament was extruded at a temperature of 230ºC using the right extruder to print the bottom electrode and top electrode. The soluble HIPS filament was extruded at a temperature of 230ºC using the middle extruder to print the temporary supporter. In order to make the polymer layers have better adhesion, the temperature of the hot bed was set to 70ºC. The layer height was set to 0.3 mm. The fill rates of the PLA structures and the conductive PLA electrodes were set to be 100%. It should be noted that the fabrication step of the spacer (Fig. 5c) and the fabrication step of the supporter (Fig. 5d) were drawn in two figures just for convenience. Since the spacer and the supporter were located at the same level, each slice is alternately 3D printed by depositing PLA in the spacer region and HIPS in the supporter region in the actual printing process. With a printing speed of 40 mm/s, the integrative 3D printing process of the 3D model of the capacitive force sensor was accomplished in approximately 35 minutes without using any additional metallization process, unloading-reloading filament process, alignment process, and assembling process.

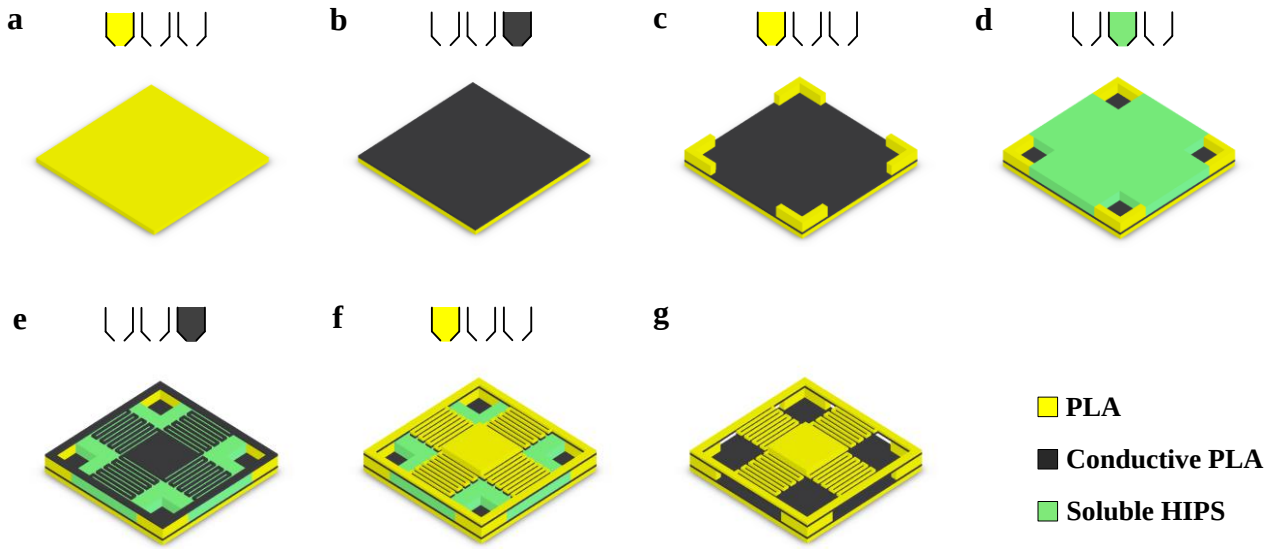

Figure 5. Illustration of the integrative 3D printing process for fabrication of the capacitive force sensor. (a) Bottom plate printing. (b) Bottom electrode printing. (c) Spacer printing. (d) Supporter printing. (e) Top electrode printing. (f) Top plate printing. (g) Removal of the HIPS supporter by D-Limonene.

Fig. 6c shows a photograph of the 3D model of the capacitive force sensor after 3D printing. After that, the 3D printed model was putted into the solvent of D-Limonene (Fig. 6a). The HIPS supporter began to dissolve in D-Limonene at room temperature (Fig. 6b). After approximately 10 hours of soaking, the HIPS supporter was completely removed. The 3D printed device was soaked and washed in ethanol and water to remove residual D-Limonene, then the capacitive force sensor with a suspended beam-plate structure was obtained. Fig. 6d shows a photograph of the capacitive force sensor fabricated by the integrative 3D printing process.

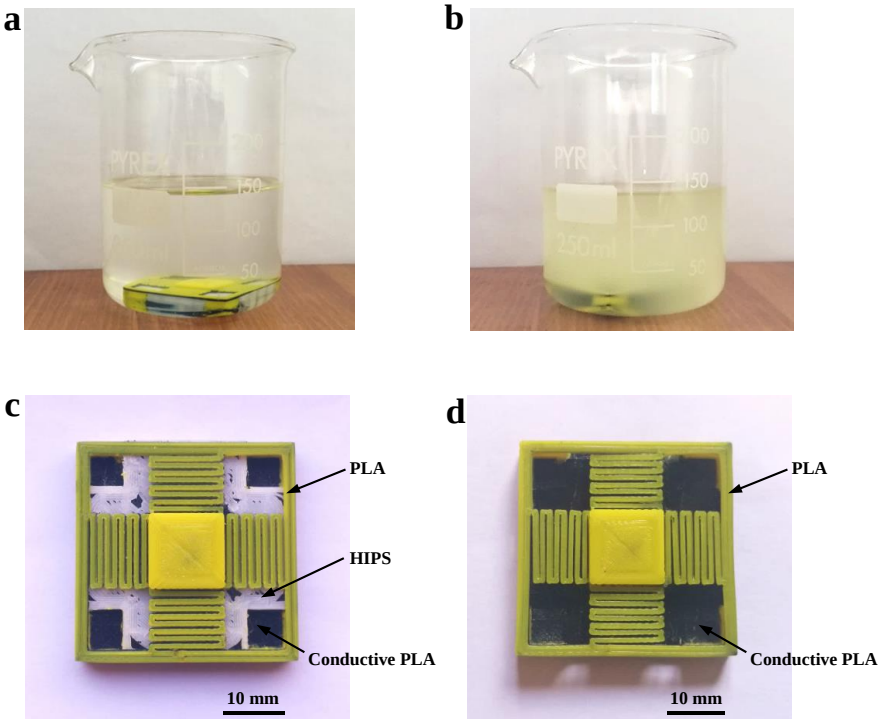

Figure 6. Photographs of the capacitive force sensor fabricated by the integrative 3D printing process. (a) The 3D printed model was putted into the solvent of D-Limonene. (b) The HIPS supporters began to dissolve in the solvent of D-Limonene. (c) Photograph of the device after 3D printing. (d) Photograph of the 3D printed device after removing the HIPS supporter.

3. Results and discussion

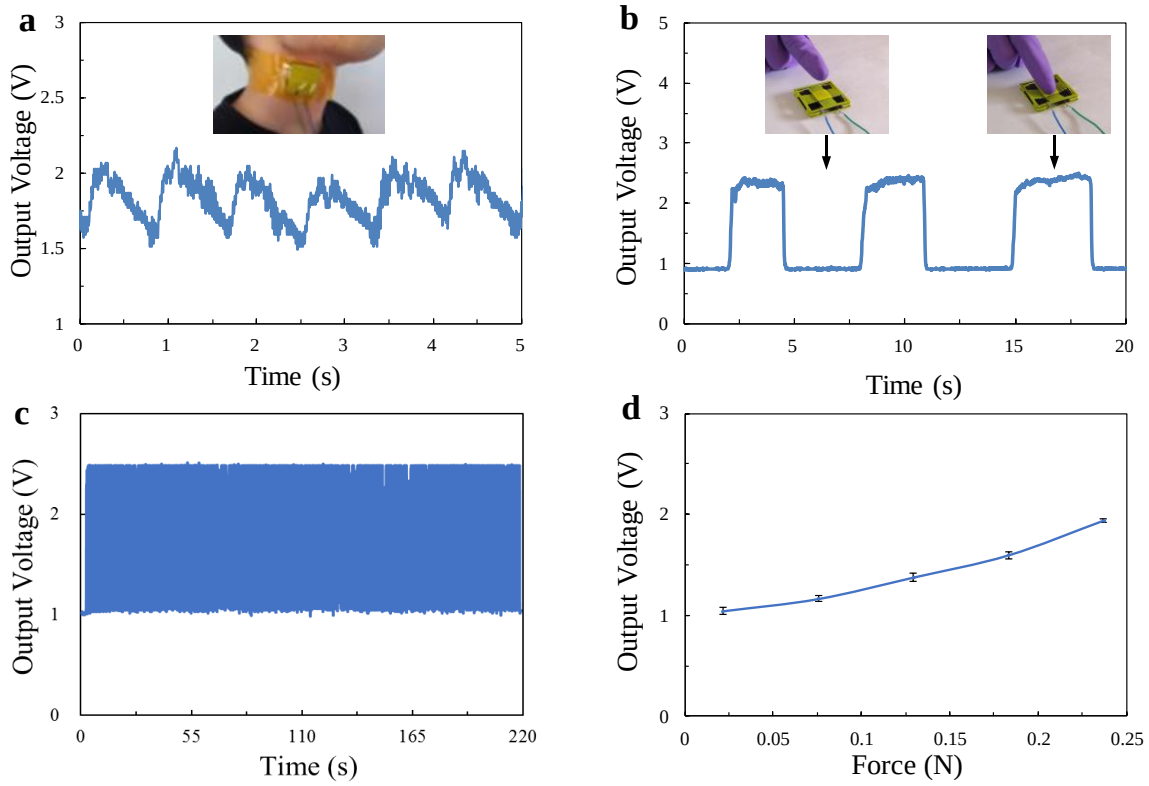

Figure 7. Measurement results of the capacitive force sensor. (a) Pulse waveform measured using the force sensor. (b) The response of the force sensor under repeated finger presses. The photograph inserts show the measurement methods. (c) Cycle test under repetitive force. (d) Relationship between the force and output voltage.

In order to measure the performances, the one-step 3D printed capacitive force sensor was connected to the capacitive readout IC MS3110, which can detect small capacitance changes and convert to output voltages. With a supply voltage of 5 V, the dynamic changes of the output voltage were recorded by a Tektronix MSO 2012 oscilloscope. When the 3D printed force sensor was attached to the neck of an adult, capacitance changes caused by the blood pulse were detected. The six complete peaks in five seconds in the waveform shown in Fig. 7a indicate that the pulse rate of the adult was approximately 72 beats per minute. Fig. 7b shows the application of the 3D printed force sensor in detecting the finger press. When a finger touched and pressed the top plate of the force sensor, the capacitance changes due to gap reduction were detected. When the finger was out of contact with the top plate of the force sensor, the output voltages returned to the baseline level. The three peaks in the waveform indicate that the finger totally touched the top plate three times in the past twenty seconds. These measurement results demonstrate that the one-step 3D printed force sensor has the potential for sensing and monitoring human's health and activities. The force sensor was tested by applying more than 900 cycles of repetitive force in 220 s by finger pressing of the movable plate of the sensor. Fig. 7c shows the results of the cycling test which indicates that the 3D printed force sensor has good reliability. The response of the sensor as the applied force was measured by placing a plastic cap loaded with small screws of known weight on the moveable plate. Each load and hence the force was controlled by the number of screws. The weight of each screw was 5.5 g. Fig. 7d shows the relationship between the force and output voltage. Table 1 shows the comparison of the 3D printed capacitive force sensors. It can be seen that with a suspended beam-plate structure, the force sensor has a high sensitivity.

Table 1: A comparison of the 3D printed capacitive force sensors

Method	Ref.	Size	Sensitivity	Material	Electrode
FDM	This work	36mm×36mm ×6.9mm	ΔV=~0.9V@0.24N (~1.9pF/N)	PLA	Carbon black-based PLA
FDM	[56]	40mm×10mm	ΔC=160fF@6.6N (0.024pF/N)	PI-ETPU	PI-ETPU
FDM	[57]	38.1mm× 38.1mm×2.8mm	0.215pF/kN (0.000215pF/N)	ABS	Copper wire
LCM	[40]	Radius 15mm	1.8pF/10^4Pa (~1.2pF/N)	Al_2O_3 ceramic	Silver nanoparticle ink

For MEMS devices with geometrically complex structures, it is very difficult to align and assemble the 3D printed components using the traditional multi-step fabrication method. However, the integrative 3D printing doesn't need additional alignment process and assembling process and provide a convenient method for additive manufacturing. With the rapid development of the 3D printing techniques, it has been reported that the pattern resolution could be improved to 10 μm or even higher [58]. Therefore, with a micro-scale pattern resolution, the deviations between the simulation and the measurement results can be reduced and more MEMS devices can be produced in future for personalized applications.

4. Conclusions

This paper has presented an integrative 3D printing method for rapid manufacturing of MEMS devices. With a triple-extruder 3D printer, the electrically insulating PLA filament, the electrically conductive PLA filament, and the soluble HIPS filament can be printed alternately in the 3D printing process. As an application of the method, a capacitive force sensor with a relatively complex suspended beam-plate structure has been successfully fabricated in a one-step 3D printing process without using any additional metallization process, unloading-reloading filament process, alignment process, and assembling process. The 3D printing process of the sensor was completed in 35 minutes and the removing of the sacrificial layer was completed in 10 hours. The measurement results show that the 3D printed force sensor has been operated successfully in monitoring human blood pulse and detection of contact forces. The work indicates that the integrative 3D printing method has the potential to be applied in rapidly personalized manufacturing for MEMS devices.

Acknowledgements

This work was partly supported by the UK Engineering and Physical Sciences Research Council (Grant EP/R024502/1). The authors would like to thank Dr. Yuepei Li, Mr. Leonard Mark and Dr. Alissa Potekhina at Heriot-Watt University for useful discussions. G.D. Liu, C.H. Wang and Z.L. Jia conceived the idea. G.D. Liu, K.X. Wang performed the experiments. All authors analyzed the data, discussed the results and commented on the manuscript.

References

[1] Hu, Q., Gao, C., Hao, Y., Zhang, Y. & Yang, G 2011 Low cross-axis sensitivity micro-gravity microelectromechanical system sandwich capacitance accelerometer *Micro Nano Lett.* **6** 510-514.

[2] G.D. Liu, W.P. Cui, H. Hu, F.S. Zhang, Y.X. Zhang, C.C. Gao, Y.L. Hao 2015 High temperature pressure sensor using a thermostable electrode *10th IEEE International Conference on Nano/Micro Engineered and Molecular Systems* 201-204.

[3] G. Liu, W. Cui, H. Hu, F. Zhang, Y. Zhang, C. Gao, Y. Hao 2015 Silicon on insulator pressure sensor based on a thermostable electrode for high temperature applications *Micro Nano Lett*. **10** 496-499.

[4] G. Liu, C. Gao, Y. Zhang, Y. Hao 2015 High temperature pressure sensor using Cu-Sn wafer level bonding *2015 IEEE SENSORS* 1-4.

[5] X. Huang, D. Zhang 2014 A high sensitivity and high linearity pressure sensor based on a peninsula-structured diaphragm for low-pressure ranges *Sens. Actuator A Phys*. **216** 176-189.

[6] C. Wei, W. Zhou, Q. Wang, X. Xia, X. Li 2012 TPMS (tire-pressure monitoring system) sensors: Monolithic integration of surface-micromachined piezoresistive pressure sensor and self-testable accelerometer *Microelectron. Eng.* **91** 167-173.

[7] J. Mai, L. Zhang, F. Tao, L. Ren 2016 Customized production based on distributed 3D printing services in cloud manufacturing *Int. J. Adv. Manuf. Technol.* **84** 71-83.

[8] B. Utela, D. Storti, R. Anderson, M. Ganter 2008 A review of process development steps for new material systems in three dimensional printing (3DP) *J. Manuf. Process.* **10** 96-104.

[9] T.D. Ngo, A. Kashani, G. Imbalzano, K.T.Q. Nguyen, D. Hui 2018 Additive manufacturing (3D printing): A review of materials, methods, applications and challenges *Compos. B. Eng*. **143** 172-196.

[10] S. Singh, S. Ramakrishna, R. Singh 2017 Material issues in additive manufacturing: A review *J. Manuf. Process.* **25** 185-200.

[11] X. Xu, P. Robles-Martinez, C.M. Madla, F. Joubert, A. Goyanes, A.W. Basit, S. Gaisford 2020 Stereolithography (SLA) 3D printing of an antihypertensive polyprintlet: Case study of an unexpected photopolymer-drug reaction, *Addit. Manuf.* **33** 101071.

[12] S.F.S. Shirazi, S. Gharehkhani, M. Mehrali, H. Yarmand, H.S.C. Metselaar, N. Adib Kadri, N.A.A. Osman 2015 A review on powder-based additive manufacturing for tissue engineering: selective laser sintering and inkjet 3D printing *Sci. Technol. Adv. Mater*. 16 033502.

[13] H. Mazhar, T. Osswald, D. Negrut 2016 On the use of computational multi-body dynamics analysis in SLS-based 3D printing *Addit. Manuf.* **12** 291-295.

[14] D.X. Luong, A.K. Subramanian, G.A.L. Silva, J. Yoon, S. Cofer, K. Yang, P.S. Owuor, T. Wang, Z. Wang, J. Lou, P.M. Ajayan, J.M. Tour 2018 Laminated Object Manufacturing of 3D-Printed Laser-Induced Graphene Foams *Adv. Mater.* **30** 1707416.

[15] Z. Wang, N. Martin, D. Hini, B. Mills, K. Kim 2017 Rapid Fabrication of Multilayer Microfluidic Devices Using the Liquid Crystal Display-Based Stereolithography 3D Printing System, 3D Print *Addit. Manuf.* **4** 156-164.

[16] F. Ning, W. Cong, J. Qiu, J. Wei, S. Wang 2015 Additive manufacturing of carbon fiber reinforced thermoplastic composites using fused deposition modeling *Compos. B. Eng.* **80** 369-378.

[17] O.A. Mohamed, S.H. Masood, J.L. Bhowmik 2017 Experimental investigation of time-dependent mechanical properties of PC-ABS prototypes processed by FDM additive manufacturing process *Mater. Lett.* **193** 58-62.

[18] S. Naghieh, M.R. Karamooz Ravari, M. Badrossamay, E. Foroozmehr, M. Kadkhodaei 2016 Numerical investigation of the mechanical properties of the additive manufactured bone scaffolds fabricated by FDM: The effect of layer penetration and post-heating *J. Mech. Behav. Biomed. Mater.* **59** 241-250.

[19] O.A. Mohamed, S.H. Masood, J.L. Bhowmik 2015 Optimization of fused deposition modeling process parameters: a review of current research and future prospects *Adv. Manuf.* **3** 42-53.

[20] S. Chohan Jasgurpreet, R. Singh 2017 Pre and post processing techniques to improve surface characteristics of FDM parts: a state of art review and future applications *Rapid Prototyp. J.* **23** 495-513.

[21] A. Rodríguez-Panes, J. Claver, A.M. Camacho 2018 The Influence of Manufacturing Parameters on the Mechanical Behaviour of PLA and ABS Pieces Manufactured by FDM: A Comparative Analysis *Materials* **11**.

[22] M. Dawoud, I. Taha, S.J. Ebeid 2016 Mechanical behaviour of ABS: An experimental study using FDM and injection moulding techniques *J. Manuf. Process.* **21** 39-45.

[23] J.M. Barrios, P.E. Romero 2019 Improvement of Surface Roughness and Hydrophobicity in PETG Parts Manufactured via Fused Deposition Modeling (FDM): An Application in 3D Printed Self–Cleaning Parts *Materials* **12**.

[24] J. Wu, N. Chen, F. Bai, Q. Wang 2018 Preparation of poly (vinyl alcohol)/poly (lactic acid)/hydroxyapatite bioactive nanocomposites for fused deposition modeling *Polym. Compos.* **39** E508-E518.

[25] M. Lay, N.L.N. Thajudin, Z.A.A. Hamid, A. Rusli, M.K. Abdullah, R.K. Shuib 2019 Comparison of physical and mechanical properties of PLA, ABS and nylon 6 fabricated using fused deposition modeling and injection molding *Compos. B. Eng.* **176** 107341.

[26] M.Á. Caminero, J.M. Chacón, E. García-Plaza, P.J. Núñez, J.M. Reverte, J.P. Becar 2019 Additive Manufacturing of PLA-Based Composites Using Fused Filament Fabrication: Effect of Graphene Nanoplatelet Reinforcement on Mechanical Properties, Dimensional Accuracy and Texture *Polymers* **11**.

[27] J. H. Hong, T. Yu, Z. Chen, S. J. Park, Y. H. Kim 2019 Improvement of flexural strength and compressive strength by heat treatment of PLA filament for 3D-printing *Mod. Phys. Lett. B* **33** 1940025.

[28] Y.C. Keat, Y.W. Yin, M.Z. Ramli, T.P. Leng, S.C. Chie 2019 Effects of infill density on the mechanical properties of 3D printed PLA and conductive PLA *AIP Conference Proceedings* **2129** 020013.

[29] S. Sundaram, M. Skouras, D.S. Kim, L. van den Heuvel, W. Matusik, 2019 Topology optimization and 3D printing of multimaterial magnetic actuators and displays *Sci. Adv.* **5** eaaw1160.

[30] O. Ulkir 2020 Design and fabrication of an electrothermal MEMS micro-actuator with 3D printing technology *Mater. Res. Express.* **7** 075015.

[31] Y. Xu, X. Wu, X. Guo, B. Kong, M. Zhang, X. Qian, S. Mi, W. Sun 2017 The Boom in 3D-Printed Sensor Technology *Sensors* **17**.

[32] H. Yang, W.R. Leow, X. Chen 2018 3D Printing of Flexible Electronic Devices *Small Methods* **2** 1700259.

[33] A. Zolfagharian, A. Kaynak, A. Noshadi, A.Z. Kouzani 2019 System identification and robust tracking of a 3D printed soft actuator *Smart Mater. Struct.* **28** 075025.

[34] S. Shin, H. So 2020 Effect of 3D printing raster angle on reversible thermo-responsive composites using PLA/ paper bilayer *Smart Mater. Struct.* **29** 105016.

[35] A.M. Tothill, M. Partridge, S.W. James, R.P. Tatam 2017 Fabrication and optimisation of a fused filament 3D-printed microfluidic platform *J. Micromech. Microeng.* **27** 035018.

[36] J. Chen, X. Liu, Q. Zhang 2020 Fast fabrication of a 3D prototyping microfluidic device for liquid cross-flow and droplet high-throughput generation *J. Micromech. Microeng.* **30** 047001.

[37] Sparks D 2019 3D-printed substrates for wafer-level and chip-scale fluidic packaging *Chip-Scale Review* **23** 42.

[38] V. Zega, C. Credi, R. Bernasconi, G. Langfelder, L. Magagnin, M. Levi, A. Corigliano 2018 The First 3-D-Printed z-Axis Accelerometers With Differential Capacitive Sensing *IEEE Sens. J.* **18** 53-60.

[39] J.J. Adams, E.B. Duoss, T.F. Malkowski, M.J. Motala, B.Y. Ahn, R.G. Nuzzo, J.T. Bernhard, J.A. Lewis 2011 Conformal Printing of Electrically Small Antennas on Three-Dimensional Surfaces *Adv. Mater.* **23** 1335-1340.

[40] L.M. Faller, W. Granig, M. Krivec, A. Abram, H. Zangl 2018 Rapid prototyping of force/pressure sensors using 3D- and inkjet-printing *J. Micromech. Microeng.* **28** 104002.

[41] M.I.M. Ghazali, S. Karuppuswami, S. Mondal, P. Chahal 2018 Embedded Active Elements in 3D Printed Structures for the Design of RF Circuits *2018 IEEE 68th Electronic Components and Technology Conference (ECTC)* 1062-1067.

[42] J. Marques-Hueso, T.D.A. Jones, D.E. Watson, A. Ryspayeva, M.N. Esfahani, M.P. Shuttleworth, R.A. Harris, R.W. Kay, M.P.Y. Desmulliez 2018 A Rapid Photopatterning Method for Selective Plating of 2D and 3D Microcircuitry on Polyetherimide *Adv. Funct. Mater.* **28** 1704451.

[43] Q. Mu, L. Wang, C.K. Dunn, X. Kuang, F. Duan, Z. Zhang, H.J. Qi, T. Wang 2017 Digital light processing 3D printing of conductive complex structures *Addit. Manuf.* **18** 74-83.

[44] P.F. Flowers, C. Reyes, S. Ye, M.J. Kim, B.J. Wiley 2017 3D printing electronic components and circuits with conductive thermoplastic filament *Addit. Manuf.* **18** 156-163.

[45] J.P. Wissman, K. Sampath, S.E. Freeman, C.A. Rohde 2019 Capacitive Bio-Inspired Flow Sensing Cupula *Sensors* **19** 11.

[46] A. Dijkshoorn, P. Werkman, M. Welleweerd, G. Wolterink, B. Eijking, J. Delamare, R. Sanders, G.J.M. Krijnen 2018 Embedded sensing: integrating sensors in 3-D printed structures *J. Sens. Sens. Syst.* **7** 169-181.

[47] A.M. Kamat, Y. Pei, B. Jayawardhana, A.G.P. Kottapalli 2021 Biomimetic Soft Polymer Microstructures and Piezoresistive Graphene MEMS Sensors Using Sacrificial Metal 3D Printing *ACS Appl. Mater. Interfaces* **13** 1094-1104.

[48] A.M. Kamat, X. Zheng, B. Jayawardhana, A.G.P. Kottapalli 2020 Bioinspired PDMS-graphene cantilever flow sensors using 3D printing and replica moulding *Nanotechnology* **32** 095501.

[49] S.J. Leigh, R.J. Bradley, C.P. Purssell, D.R. Billson, D.A. Hutchins 2012 A Simple, Low-Cost Conductive Composite Material for 3D Printing of Electronic Sensors *PLOS ONE* **7** e49365.

[50] J.R. McGhee, M. Sinclair, D.J. Southee, K.G.U. Wijayantha 2018 Strain sensing characteristics of 3D-printed conductive plastics *Electron. Lett.* **54** 570-572.

[51] K. Angel, H.H. Tsang, S.S. Bedair, G.L. Smith, N. Lazarus 2018 Selective electroplating of 3D printed parts *Addit. Manuf.* **20** 164-172.

[52] M.J. Kim, M.A. Cruz, S. Ye, A.L. Gray, G.L. Smith, N. Lazarus, C.J. Walker, H.H. Sigmarsson, B.J. Wiley 2019 One-step electrodeposition of copper on conductive 3D printed objects *Addit. Manuf.* **27** 318-326.

[53] Lyshevski, S. E. 2004 MEMS and NEMS - systems, devices, and structures *IEEE Electr. Insul. Mag.* **20** 46-46.

[54] V. Zega, M. Invernizzi, R. Bernasconi, F. Cuneo, G. Langfelder, L. Magagnin, M. Levi, A. Corigliano 2019 The First 3D-Printed and Wet-Metallized Three-Axis Accelerometer With Differential Capacitive Sensing *IEEE Sens. J.* **19** 9131-9138.

[55] N.J. Castro, R. Patel, L.G. Zhang 2015 Design of a Novel 3D Printed Bioactive Nanocomposite Scaffold for Improved Osteochondral Regeneration *Cell. Mol. Bioeng.* **8** 416-432.

[56] M. Schouten, R. Sanders, G. Krijnen 2017 3D printed flexible capacitive force sensor with a simple micro-controller based readout *2017 IEEE SENSORS* 1-3.

[57] M. Saari, B. Xia, B. Cox, P.S. Krueger, A.L. Cohen, E. Richer 2016 Fabrication and Analysis of a Composite 3D Printed Capacitive Force Sensor *3D Print. Addit. Manuf.* **3** 136-141.

[58] B. Zhang, B. Seong, V. Nguyen, D. Byun 2016 3D printing of high-resolution PLA-based structures by hybrid electrohydrodynamic and fused deposition modeling techniques *J. Micromech. Microeng.* **26** 025015.